Appendix DR1

Marine osmium isotopic record across the Triassic–Jurassic boundary from a Pacific pelagic site

Junichiro Kuroda[1,2*], Rie S. Hori[3], Katsuhiko Suzuki[1], Darren R. Gröcke[4], and Naohiko Ohkouchi[1]

[1]*Japan Agency for Marine-Earth Science and Technology, Yokosuka 237-0061, Japan*
[2]*National Oceanography Centre, Southampton, University of Southampton, SO14 3ZH, UK*
[3]*Graduate School of Science, Ehime University, Matsuyama 790-8577, Japan*
[4]*Department of Earth Sciences, Durham University, Durham, DH1 3LE, UK*
*Author for correspondence: kurodaj@jamstec.go.jp

DESCRIPTION OF ANALYTICAL METHOD

Rhenium and Osmium Analyses

Prior to analysis, each sample was crushed to coarse fragments, from which we handpicked fresh fragments without veins, nodules, or weathered surfaces. The fresh fragments were ultrasonically washed with dilute HNO_3, rinsed 3–5 times with Milli-Q water, and then heated to dryness. Each sample was then crushed in an alumina mill.

Re and Os were extracted from chert samples using inverse aqua regia digestion. We consider that platinum group elements extractable from chert using this method are mainly from hydrogenous components; i.e., Re and Os absorbed on Fe-Mn oxides and hydroxides, as well as on organic matter. After spiking the samples with solutions enriched in ^{190}Os and ^{185}Re, 5–8 g of powdered sample was sealed in a Carius tube (**Shirey and Walker, 1995**) with 10 ml of the digestion solution, and heated at 230°C for 24 hr. Os was then separated from the leachate using CCl_4 extraction (**Cohen and Waters, 1996**; **Pearson and Woodland, 2000**) and subsequent microdistillation using a modified version of the method described by **Roy-Barman (1993**) (see **Kato et al., 2005**). Re was separated from the aqueous phase using Bio-Rad AG1-X8 anion exchange resin (100-200 mesh).

Abundances of Re and Os and Os isotope contents were analyzed using a negative thermal

ionization-mass spectrometry (Thermo Electron TRITON) at JAMSTEC, Japan, with each batch of samples measured along with in-house Re and Os standards. Raw Re and Os oxide values were corrected for oxygen isotope contribution and mass fractionation. The Re and Os isotopic values and elemental abundances are calculated by full propagation of uncertainties from Re and Os mass spectrometer measurements, blank abundance and isotopic composition, and spike calibration. Total procedural blanks for Re and Os are 9-40 and 3-6 pg, respectively, with an average $^{187}Os/^{188}Os$ value of ~0.17 (n = 4). All data were corrected for the procedural blank for each analytical batch (see Table DR1). The magnitude of the blank correction for Os and Re concentrations was typically 6–15% and 3–20%, respectively. Instrument reproducibility was monitored based on replicate analyses of the in-house standard for $^{187}Os/^{188}Os = 0.10664 \pm 0.00044$ (2σ). The Re standard runs produced average $^{185}Re/^{187}Re$ values of 1.6749 ± 0.0040 (2σ) identical to the reported value of 1.6755 ± 0.0014 (2σ) (**Suzuki et al., 2004**).

The average values of $^{187}Os/^{188}Os$ and $^{187}Re/^{188}Os$ measured for the rock reference material JCh-1 (chert) issued by Geological Survey of Japan (http://riodb02.ibase.aist.go.jp/geostand/) were 0.606 ± 0.044 and 17.2 ± 4.9 (2σ, n = 5), respectively. The average concentrations of Re and Os of JCh-1 are 17.3 ± 4.8 and 5.71 ± 0.79 pg g^{-1} (2σ, n = 5), respectively.

Initial Os isotopic compositions ($^{187}Os/^{188}Os_i$) are calculated for the time of deposition based on the measured $^{187}Os/^{188}Os$ and $^{187}Re/^{188}Os$ values, and the age of the Triassic and Jurassic boundary (200 Ma; **Ogg et al., 2008**) and the ^{187}Re decay constant of $\lambda = 1.666 \times 10^{-11}$ a^{-1} (**Smoliar et al., 1996**). The calculated initial is taken to represent the seawater $^{187}Os/^{188}Os$ composition at the time of sediment deposition.

Because the age of deposition for JCh-1 has been roughly estimated to be Triassic, we calculated $^{187}Os/^{188}Os_i$ values for JCh-1 by assuming the onset (253 Ma) and the end of Triassic (200 Ma), which were 0.541 ± 0.052 and 0.555 ± 0.050 (2σ, n = 5), respectively. Therefore, the uncertainty in the calculated $^{187}Os/^{188}Os_i$ is likely around 0.050-0.052 (2σ).

Although the chert succession investigated in this study range from end-Norian (~204 Ma) through Triassic/Jurassic boundary (199.6 Ma) to mid-Sinemurian (~193 Ma), differences in $^{187}Os/^{188}Os_i$ values between 204 and 194 Ma are typically smaller than 0.01 (<3%), because of low $^{187}Re/^{188}Os$ ratios (<70). It indicates that uncertainty associated with the age of sediments is negligible.

Carbon Isotope Analysis

Carbon isotope analysis was conducted on decalcified bulk sediment using 3 M HCl in 50 ml centrifuge tubes for 16 h. Stable isotope measurements were performed at Durham using a Costech EA coupled to a ThermoFinnigan Delta V Advantage. Carbon-isotope ratios are corrected for ^{17}O contribution (**Craig, 1957**) and reported in standard delta (δ) notation in per mil (‰) relative to the VPDB scale. Data accuracy is monitored through routine analyses of in-house standards, which are stringently calibrated against international standards. Analytical uncertainty for $\delta^{13}C_{org}$ measurements is typically better than ±0.1‰ for standards and <0.2‰ on replicate sample analysis. Total organic carbon (TOC) data was obtained as part of this method. Because of the low TOC contents of these chert samples, the tin capsules used contained up to 100–120 mg of chert powder, and the Costech EA was set to Macro-O_2. The isotopic analyses were done in no dilution mode and all results shown produced more than 1V.

BIOSTRATIGRAPHY

Radiolaria and conodont are useful fossils for age-determination of this Kurusu section because no other diagnostic fossils have been obtained from this deep-sea sequence. Radiolarian biostratigraphy of this section has been documented by **Hori (1988, 1990, 1992)** and **Hori et al (2007)**. A preliminary stratigraphic study of conodont has been performed by **Iwabu and Hori (2004)**. Here, we re-examined the final and first occurrences of conodont and radiolarian species

close to the Triassic–Jurassic boundary horizons (**Fig. DR1**).

Radiolarian Biostratigraphy

Three radiolarian biozones (*Canoptum triassicum*, *Pantanellium tanuense*, and *Parahsuum simplum* Zones in ascending order) are recognized for bedded chert succession investigated in this study (**Figs. 1** and **DR1**). The uppermost Triassic radiolarian zone (*C. triassicum*) in this site is further divided into three subzones: *Betraccum deweveri*, *Haeckelicyrtium breviora*, and *Globolaxtorum tozeri* Subzones (**Hori, 2002**; **Carter and Hori, 2005**). The *B. deweveri* and *G. tozeri* Subzones are well correlative to those from Queen Charlotte Islands (QCI), British Columbia, Canada (**Carter, 1993**). According to **Carter (1993)**, the *B. deweveri* Subzone is correlated to the *cordilleranus* ammonite zone, which corresponds to Norian stage. Although the definition of Norian-Rhaetian boundary is still controversial, and the first occurrence of *Misikella posthernsteini* in this section is observed far above (around -8 cm level), we tentatively identify the Norian-Rhaetian boundary at the top of the *B. deweveri* Subzone (-2.6 m level). The lower Jurassic *Pantanellium tanuense* Zone of this site can be directly correlated to four radiolarian zones in the QCI section (i.e., *Canoptum merum*, *Protokatroma aquila*, *Pantanellium browni* and *Crucella hettangica* Zones) as shown in **Hori et al. (2007)**. These radiolarian zones in QCI section correspond to the Hettangian through the lower part of Sinemurian (**Carter et al. 1998**; **Longridge et al. 2007**). In Kurusu section, the Hettangian-Sinemurian boundary is approximately +1.4 m level, where *Pantanellium tanuense* marks its final occurrence below the first occurrence of *Parahsuum simplum*. The species *P. tanuense*, is considered as one of the diagnostic radiolarian taxa of Hettangian stage and became extinct around Hettangian-Sinemurian boundary (**Pessagno and Blome 1980**; **Carter et al. 1998**). On the contrary, the first occurrence of *Parahsuum simplum* locates in lower Middle Sinemurian based on the radiolarian biostratigraphic data comparing with ammonite zones in QCI (**Carter et al. 1998**). Taking these facts into consideration, we identify the Hettangian-Sinemurian

boundary at the uppermost part of *Pantanellium tanuense* Zone in the Kurusu section, beneath the base of *Parahsuum simplum* Zone.

Conodont biostratigraphy and the Triassic–Jurassic boundary

Successive occurrences of conodont species such as *Misikella hernsteini*, *M. aff. hernsteini* and *M. posthernsteini* are recognized in the interval from -20 to +28 cm of the Kurusu section. None of any specimen of *Misikella ultima* has been obtained from this section. The final occurrence horizon of conodont fossils is located in +28 cm, where *Pantanellium tanuense* also occur (**Fig. DR1**). As discussed above, *P. tanuense* is an index radiolarian taxon of the Hettangian stage, however, *P.* cf. *tanuense* is recognized in the -8 cm level, where *M. posthernsteini* occur with rich Rhaetian radiolarian fauna. In addition, *M. hernsteini* marks its final occurrence just below the -8 cm level. Hence, the -8 cm level is not regarded to be Hettangian, but should be identified as the Rhaetian stage.

It is difficult to determine the exact position of the Triassic–Jurassic (T–J) boundary based on the present micropaleontological data, but we can tentatively identify the T–J boundary somewhere between +28 cm (the highest occurrence level of conodont) and +48 cm levels, where several species of Jurassic type Bipedis such as *B. hannai* and *B. elizabethae* occur (**Fig. DR1**). Here we regard this interval as the T–J boundary zone. Except for *Pantanellium tanuense*, no diagnostic radiolarian taxa for stratigraphic index such as *Tipperella kennecottensis* (an index marker of T–J boundary; **Longridge et al., 2007**) was observed in the T–J boundary zone. The T–J boundary zone is characterized by extremely rich spherical spumellarians.

REFERENCES CITED

Carter, E.S., 1993, Biochronology and Paleontology of uppermost Triassic (Rhaetian) radiolarians, Queen Charlotte Islands, British Columbia, Canada: Mémoires de Géologie (Loausanne), v. 11,

175 p.

Carter, E.S., and Hori, R.S., 2005, Global correlation of the radiolarian faunal change across the Triassic-Jurassic boundary: Canadian Journal of Earth Sciences, v. 42(5), p. 777-790.

Carter, E.S., Whalen, P.A., and Guex, J., 1998, Biochronology and paleontology of Lower Jurassic (Hettangian and Sinemurian) radiolarians, Queen Charlotte Islands, British Columbia: Geological Survey of Canada Bulletin, v. 496, 162 p.

Cohen, A.S., and Waters, G.G., 1996, Separation of osmium from geological materials by solvent extraction for analysis by thermal ionization mass spectrometry: Analytica Chimica Acta, v. 332, p. 269–275.

Craig, H., 1957, Isotopic standards for carbon and oxygen and correction factors for mass-spectrometric analysis of carbon dioxide: Geochimica et Cosmochimica Acta, v. 12, p. 133–149.

Hori, R., 1988, Some characteristic radiolarians from Lower Jurassic bedded cherts of the Inuyama area, southwest Japan: Transactions and Proceedings of the Palaeontological Society of Japan, N.S. 151, p.543-563.

Hori, R., 1990, Lower Jurassic radiolarian zones of southwest Japan: Transactions and Proceedings Palaeontological Society of Japan, N.S. 159, p.562-585.

Hori, R., 1992, Radiolarian biostratigraphy at the Triassic/Jurassic period boundary in bedded cherts from the Inuyama area, central Japan: Journal of Geosciences, Osaka City University, v.35, p. 53-65.

Hori, R., 2002, Lower Jurassic radiolarian zones and IGCP458 (Triassic/Jurassic boundary event): Proceedings with programs, Pre-symposium of the 109th annual meeting of the Geological Society of Japan, p.47-52 (in Japanese).

Hori, R.S., Fujiki, T., Inoue, E., and Kimura, J.-I., 2007, Platinum group element anomalies and bioevents in the Triassic-Jurassic deep-sea sediments of Panthalassa: Palaeogeography,

Palaeoclimatology, Palaeoecology, v. 244, p. 391-406, doi:10.1016/j.palaeo.2006.06.038.

Iwabu, M., and Hori, R.S., 2004, A clastic rock layer in latest Triassic bedded chert from Inuyama area, Mino Terrane, Japan: Abstracts of the 153rd regular meeting, the Palaeontological Society of Japan, v. 64 (in Japanese).

Kato, Y., Fujinaga, K., and Suzuki, K., 2005, Major and trace element geochemistry and Os isotopic composition of metalliferous umbers from the Late Cretaceous Japanese accretionary complex: Geochemistry, Geophysics, Geosystems, v. 6, Q07004, doi: 10.1029/2005GC000920.

Longridge, L.M., Carter, E.S., Smith, P.L., and Tipper, H.W., 2007, Early Hettangian ammonites and radiolarians from the Queen Charlotte Islands, Brithish Columbia and their bearing on the definition of the Triassic-Jurassic boundary: Palaeogeography, Palaeonclimatology, Palaeoecology, v. 244, p. 142-169, doi:10.1016/j.palaeo.2006.06.027.

Ogg, J.G., Ogg G., and Gradstein, F.M., 2008, The Concise Geologic Time Scale: Cambridge University Press.

Pearson, D.G., and Woodland, S.J., 2000, Solvent extraction/anion exchange separation and determination of PGEs (Os, Ir, Pt, Pd, Ru) and Re-Os isotopes in geological samples by isotope dilution ICP-MS: Chemical Geology, v. 165, p. 57-107.

Pessagno, E.A., and Blome, C.D., 1980, Upper Triassic and Jurassic Pantanelliidae from Calfornia, Oregon and British Columbia: Micropaleontology, v. 26, p.225-273.

Roy-Barman, M., 1993, Mesure du rapport $^{187}Os/^{188}Os$ dans les basaltes et les péridotites: Contribution à la systematique ^{187}Re-^{187}Os dans le manteau: Ph.D. thesis, Univ. de Paris VII, Paris.

Shirey, S.B., and Walker, R.J., 1995, Carius tube digestion for low-blank rhenium-osmium analysis: Analytical Chemistry, v. 67, p. 2136–2141.

Smoliar, M.I., Walker R.J., and Morgan, J.W., 1996, Re–Os ages of group IIA, IIIA, IVA, and IVB iron meteorites: Science, v. 23, p. 1099–1102.

Suzuki, K., Miyata, Y., and Kanazawa, N., 2004, Precise Re isotope ratio measurements by negative thermal ionization mass spectrometry (NTI-MS) using total evaporation technique: International Journal of Mass Spectrometry, v. 235, p. 97–101.

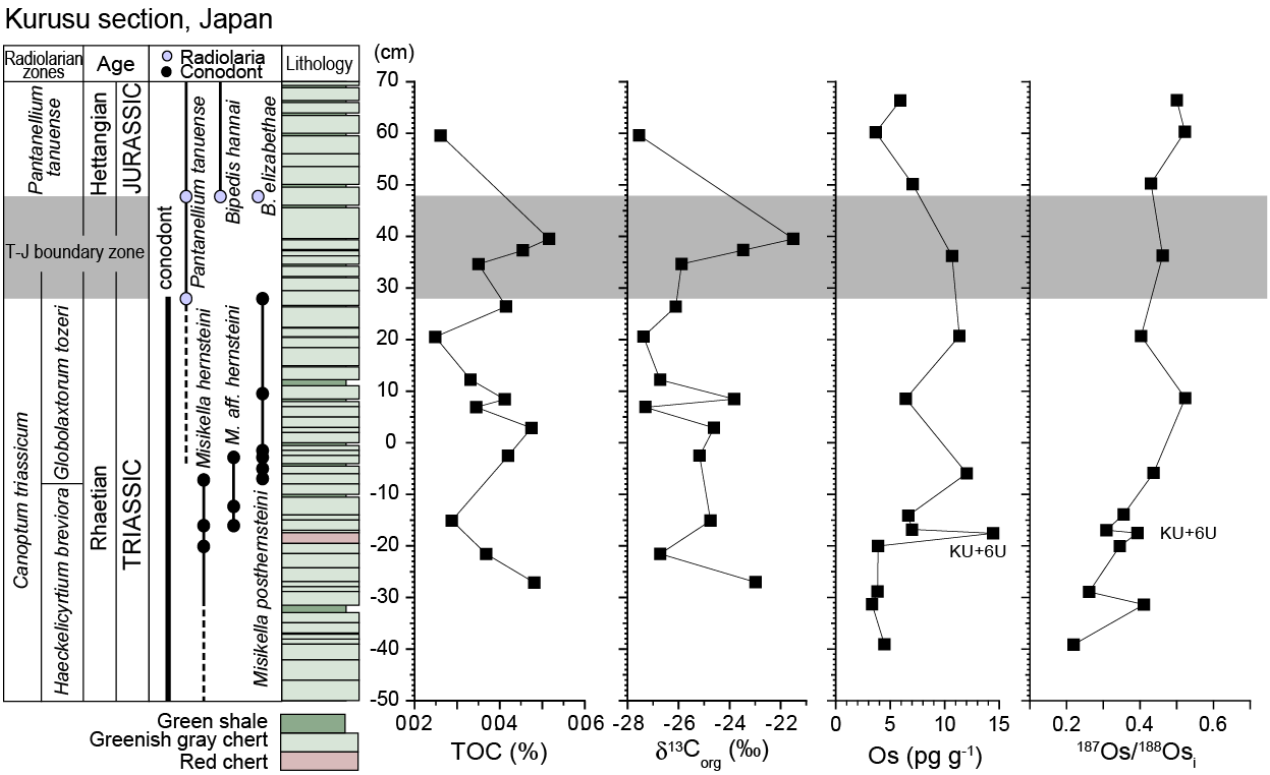

Figure DR1. Closed-up depth profiles of total organic carbon (TOC), stable isotopic ratios of total organic carbon ($\delta^{13}C_{org}$), Os abundances, and $^{187}Os/^{188}Os_i$ values around the T–J boundary, together with graphic lithology and occurrences of marine microfossils (radiolaria and conodonts). Horizontal gray band is the T–J boundary zone. The graphic lithology is after **Hori et al. (2007)**. KU+6U is a sample characterized by high abundances of platinum group elements such as Ir (**Hori et al., 2007**).

Table DR1a. Measured $^{187}Os/^{188}Os$ ratios, abundances of Os and Re, and age corrected $^{187}Os/^{188}Os$ ratios.

Sample	Position (m)	Age	Batch	$^{187}Os/^{188}Os$ measured	2SE	Os (pg g^{-1})	2SE	Re (pg g^{-1})	2SE	$^{187}Os/^{188}Os_i$ t = 200 Ma
ku+132	4.403	Jurassic	A	0.467	0.007	5.44	0.06	8.50	0.03	0.441
ku+120	4.056	Jurassic	B	0.463	0.002	3.75	0.01	5.14	0.02	0.440
ku+85	2.572	Jurassic	C	0.642	0.003	5.64	0.02	71.7	0.13	0.425
ku+75	2.073	Jurassic	C	0.651	0.002	5.43	0.02	64.6	0.12	0.448
ku+62	1.378	Jurassic	A	0.683	0.005	4.89	0.04	11.4	0.04	0.643
ku+55	1.107	Jurassic	B	0.627	0.002	3.22	0.01	13.3	0.04	0.557
ku+49	0.894	Jurassic	D	0.475	0.001	5.07	0.02	10.5	0.02	0.441
ku+45	0.728	Jurassic	D	0.557	0.003	4.03	0.03	9.58	0.02	0.517
ku+43	0.663	Jurassic	D	0.669	0.003	5.62	0.02	60.0	0.11	0.487
ku+41	0.601	Jurassic	A	0.526	0.001	3.43	0.00	1.66	0.02	0.518
ku+38	0.501	Jurassic	D	0.650	0.003	6.67	0.04	91.7	0.17	0.415
ku+34	0.362	Boundary	D	0.483	0.001	10.1	0.05	14.5	0.03	0.459
ku+28	0.206	Triassic	D	0.504	0.003	10.7	0.08	69.5	0.13	0.395
ku+23	0.085	Triassic	A	0.614	0.002	6.10	0.01	35.3	0.08	0.515
ku+14	-0.060	Triassic	B	0.576	0.002	11.4	0.04	100	0.18	0.428
ku+11	-0.140	Triassic	A	1.062	0.004	6.30	0.04	264	0.61	0.313
ku+7	-0.170	Triassic	B	0.310	0.002	6.61	0.03	0.00	0.01	0.310
ku+6U	-0.175	Triassic	D	0.420	0.002	13.7	0.07	22.6	0.04	0.393
ku+6	-0.200	Triassic	A	0.345	0.003	3.65	0.02	0.00	0.01	0.345
ku+2	-0.289	Triassic	B	0.271	0.001	3.63	0.02	2.43	0.02	0.260
ku+1	-0.314	Triassic	A	0.411	0.003	3.16	0.02	0.00	0.01	0.411
ku-4	-0.391	Triassic	B	0.236	0.001	4.18	0.02	4.78	0.02	0.218
ku-8	-0.566	Triassic	A	0.392	0.003	4.20	0.02	25.0	0.06	0.294
ku-14	-0.835	Triassic	B	0.461	0.002	3.52	0.01	22.7	0.05	0.354
ku-19	-1.047	Triassic	A	0.439	0.004	2.06	0.01	10.8	0.03	0.352
ku-22	-1.131	Triassic	B	0.423	0.006	1.58	0.01	0.00	0.01	0.423
ku-33	-1.569	Triassic	A	0.506	0.004	2.24	0.01	5.66	0.03	0.464
ku-50	-2.204	Triassic	C	0.778	0.005	3.06	0.02	38.0	0.07	0.564
ku-52	-2.229	Triassic	C	0.713	0.002	4.41	0.01	48.0	0.09	0.526
ku-60	-2.459	Triassic	C	0.659	0.004	3.82	0.02	47.4	0.09	0.447
ku-67	-2.649	Triassic	C	0.658	0.004	2.86	0.02	6.26	0.02	0.621
ku-70	-2.759	Triassic	C	0.665	0.003	4.22	0.02	26.4	0.05	0.558
ku-75	-2.854	Triassic	C	0.637	0.003	5.55	0.03	11.2	0.02	0.603
ku-78	-2.934	Triassic	C	0.705	0.003	2.00	0.01	8.75	0.02	0.630
ku-90	-3.200	Triassic	C	0.611	0.002	3.83	0.02	10.4	0.02	0.566

Table DR1b. Measured $^{187}Os/^{188}Os$ ratios, abundances of Os and Re, and age corrected $^{187}Os/^{188}Os$ ratios for JCh-1.

Sample	Split	Position	Batch	$^{187}Os/^{188}Os$ measured	2SE	Os (pg g^{-1})	2SE	Re (pg g^{-1})	2SE	$^{187}Os/^{188}Os_i$ t = 200 Ma	t = 253 Ma
JCh-1	S2	P33-1	A	0.591	0.003	5.75	0.04	21.6	0.04	0.527	0.511
JCh-1	S2	P33-1	A	0.618	0.003	5.52	0.03	14.3	0.04	0.574	0.563
JCh-1	S2	P33-1	B	0.624	0.002	5.20	0.02	16.3	0.04	0.570	0.556
JCh-1	S2	P33-1	B	0.617	0.003	5.47	0.03	17.9	0.04	0.561	0.546
JCh-1	S1	P6-5	C	0.620	0.006	6.30	0.04	16.6	0.04	0.576	0.564
JCh-1	S1	P27-3	D	0.568	0.003	5.99	0.04	17.0	0.04	0.520	0.507
JCh-1 (Average)				0.606		5.71		17.3		0.555	0.541
2S.D. (n= 6)				0.044		0.79		4.8		0.050	0.052
2R.S.D. (n = 6)				7.3%		14%		28%		8.9%	9.5%

Table DR1c. $^{187}Os/^{188}Os$ isotopic ratios and abundances of Os and Re of procedural blank for each analytical batch.

Sample	Batch	$^{187}Os/^{188}Os$	2SE	Os (pg)	Re (pg)
Procedural blank A	A	0.185	0.006	3.22	42.6
Procedural blank B	B	0.178	0.003	3.59	24.0
Procedural blank C	C	0.156	0.002	3.78	18.5
Procedural blank D	D	0.168	0.002	5.24	9.9
Blank (Average)		0.171		4.20	23.7
2R.S.D.		14%		45%	117%